

1 DOI: 10.1002/((please add manuscript number))

2 **Article type: Communication**

3
4
5 **Energy Level Alignment at Metal/Solution-Processed Organic Semiconductor Interfaces**

6
7 *Ainhoa Atxabal, Slawomir Braun, Thorsten Arnold, Xiangnan Sun, Subir Parui, Xianjie Liu,*
8 *Cristian Gozalvez, Roger Llopis, Aurelio Mateo-Alonso, Felix Casanova, Frank Ortmann,*
9 *Mats Fahlman, Luis E. Hueso**

10
11 A. Atxabal, Dr. S. Parui, Roger Llopis, Prof. F. Casanova, Prof. L. E. Hueso
12 CIC nanoGUNE, 20018 Donostia-San Sebastian, Basque Country, Spain
13 E-mail: l.hueso@nanogune.eu

14
15 Dr. S. Braun, Dr. X. Liu, Prof. M. Fahlman
16 Linköping University, 58183 Linköping, Sweden

17
18 Dr. T. Arnold, Dr. F. Ortmann
19 Institute for Materials Science, Dresden University of Technology, 01062 Dresden, Germany

20
21 Prof. X. Sun
22 CAS Center for Excellence in Nanoscience, Key Laboratory of Nanosystem and Hierarchical
23 Fabrication, National Center for Nanoscience and Technology, Beijing 100190, P. R. China

24
25 C. Gozalvez, Prof. A. Mateo-Alonso
26 POLYMAT, University of the Basque Country UPV/EHU, 20018 Donostia-San Sebastian,
27 Basque Country, Spain

28
29 Prof. A. Mateo-Alonso, Prof. F. Casanova, Prof. L. E. Hueso
30 IKERBASQUE, Basque Foundation for Science, 48013 Bilbao, Basque Country, Spain

31
32
33 **Keywords:** Hot electron transistor, spectroscopy, energy barrier, polymer, organic electronics
34

43
44 The optimization of the performance of organic-based devices such as organic photovoltaic
45 cells (OPV), organic light emitting diodes (OLED) and organic field effect transistors (OFET)
46 has been the subject of intensive research over the past twenty years.^[1-4] Due to such research
47 efforts, the key role of the energy barriers built up between the metal Fermi level and the
48 molecular levels devoted to charge transport for the device performance has been
49 elucidated.^[5-7] Typically, techniques such as electron photoemission spectroscopy, Kelvin
50 probe measurements and in-device hot electron spectroscopy have been applied to the study
51 of interfacial energy barriers.^[8-13] The first two methods are limited to extract the energy
52 level alignment by monitoring the change in the work function for thin molecular layers
53 evaporated on the surface of a metal. They require complex equipment and are far from being
54 implemented into device architecture. The third method, hot electron spectroscopy, has
55 however opened the possibility to determine energy barriers between a metal and an organic
56 semiconductor without using any material parameters and in-device operative conditions.^{[12,}
57 ^{13]} This advantage occurs by the ability of monitoring the current flow in a three-terminal
58 device, which is directly related with metal/semiconductor charge injection energy barriers.
59 However, challenges and questions still remain regarding to this last technique. Consequently,
60 in this article we would like to tackle a two-fold problem.

61
62 On the one side, hot electron devices have not yet been demonstrated in *ex-situ* fabrication
63 conditions with polymers. These materials are closer to industrial applications for plastic
64 electronics (OPV, OLED, OFET, etc.) than many small molecules considering that they can
65 be processed over large areas at low cost. Establishing this method as a quick, direct
66 procedure for the measurement of the metal/polymeric semiconductor energy barrier could be
67 of great interest. So far there are no suitable methods that enable the measurement of
68 metal/lowest unoccupied molecular orbital (LUMO) interfaces when dealing with polymers.

69 The most powerful one is probably inverse photoemission electron spectroscopy (IPES).^[14]
70 However, its low resolution and the damage it creates to the organic film by exposing the
71 sample to energetic electrons limits its use only to well-established small molecules such as
72 C₆₀ or 3,4,9,10-Perylentetracarbonsäuredianhydrid (PTCDA).^[14] On the other side, from a
73 more basic point of view, there are still concerns regarding the effects of impurity layers
74 consequence of *ex-situ* fabrication techniques on the energy barrier alignment between the
75 metal and the organic semiconductor and thus, on the charge injection into the semiconductor.
76 A device approach is hence required to solve this question, which ramifies the field of organic
77 electronics from fundamental understanding to industrial applications.

78
79 In this communication we measure the interfacial energy barrier between metals and the
80 solution processed electron-transporting polymer, poly{[N, N'-bis(2-octyldodecyl)-
81 naphthalene-1,4,5,8-bis(dicarboximide)-2,6-dyl]-*alt*-5,5'-(2,2'-dithiophene)}[P(NDI2OD-T2),
82 PolyeraActivInkTM N2200] by using in-device hot-electron spectroscopy.^[15] We chose this
83 particular polymer due to its high electron mobility and stability under ambient conditions,
84 which have led to promising technological applications.^[15-17] The devices were fabricated by
85 spin coating the polymer solution in air, i.e. far from ideal ultra clean conditions that are
86 obtained with *in-situ* evaporation, but also potentially cheaper and scalable.

87
88 Our novel results regarding the interfacial energy barrier and the role of the *ex-situ* created
89 contamination layer between the metal and the polymer are supported by standard ultraviolet
90 photoemission spectroscopy (UPS) measurements.^[9] Contrary to IPES, UPS is an indirect
91 method as it can only probe occupied states and diverse approximations must be done for
92 reaching a metal/LUMO energy value. However, the damage produced in the organic film and
93 the low resolution obtained with the former method have made UPS a more suitable technique
94 for the extraction of metal/LUMO energy barriers. The data is complemented with the

95 development of a theoretical model, which reconciles the electron photoemission results with
96 those coming from electrical transport. This work gives a further understanding of the energy
97 barriers built up between metals and polymeric semiconductors considering realistic
98 interfaces while demonstrating the power and potential of the in-device hot electron
99 spectroscopy for the determination of these energy barriers.

100

101 The first method we have used for the extraction of metal/solution processed organic
102 semiconductor interface energy barriers is in-device hot electron spectroscopy. Although this
103 technique was first applied for the determination of the energy level alignment at
104 metal/inorganic semiconductor and metal/small molecule semiconductor interfaces, in this
105 work, for the first time, we use in-device hot-electron spectroscopy for the determination of
106 energy barriers between a metal and a polymeric semiconductor.^[10, 18, 12, 13] The working
107 principle is shown in **Figure 1**. In more detail, our three-terminal device is composed of an
108 emitter, a base and a collector. The emitter is a 13 nm-thick aluminum contact, which later is
109 plasma-oxidized *in-situ* to create an AlO_x tunnel barrier. 10 nm of gold are evaporated as base
110 contact. Gold was chosen for being a commonly used material for device contacts. Its air
111 stability and noble properties make it a suitable metal for, among others, pre-patterned devices.
112 This emitter-base sample is spin coated with a solution of N2200 (see Experimental Section)
113 in ambient conditions inside the clean room. The polymer is the collector of the system. A 13-
114 nm-thick Al top electrode is used to receive the collector current from the semiconductor. In
115 these devices, the energy level alignment between the Fermi level of emitter and base is
116 externally controlled with a bias between emitter and base V_{EB} (see Figure 1), while the
117 energy alignment at the base/collector interface is naturally given by the metal/polymer
118 energy barrier Δ .

119

120 When a negative bias V_{EB} is applied a current I_E is injected from the emitter into the device by
121 tunneling through the AlOx barrier. These electrons are “hot” in the base as their energy is
122 above the Fermi energy of the metal, and a fraction of them cross the base ballistically
123 without energy attenuation.^[19] If the applied external voltage V_{EB} is lower than the barrier Δ ,
124 the ballistic electron current is reflected at the Au/N2200 interface and no collector current is
125 measured ($I_{C-hot}=0$) since it will flow instead into the base terminal (I_B). On the contrary, if
126 V_{EB} is higher than the barrier Δ (Figure 1), some of the hot electrons enter in the LUMO level
127 of N2200, diffuse towards the top Al electrode and a current is measured in the collector (I_{C-}
128 $hot \neq 0$). We point out that since N2200 is an n-type semiconductor, we measure the energy
129 barrier between the Fermi level of the gold base and the LUMO of the polymer, which is the
130 one devoted to the charge transport. Since the base electrode is kept at ground potential
131 (Figure 1), V_{EB} must be negative to inject hot electrons from the emitter into the base and then
132 to the polymer layer. Importantly, the current I_{C-hot} is measured without any external applied
133 bias between the base and collector and thus, I_{C-hot} can be considered as a purely diffusive
134 current. This is possible due to both the momentum of the injected electrons perpendicular to
135 the Au/N2200 interface and to the built-in potential created by sandwiching the polymer with
136 two metallic contacts with different work functions.^[20, 21]

137
138 Figure 2 shows the typical characterization of the device for temperatures from 290 K to 110
139 K. The I_E - V_{EB} characteristics of the tunnel junction (Al/AlOx/Au stack) are shown in Figure
140 2a. The resistance slightly increases when lowering the temperature as expected for non-leaky
141 tunnel junction.^[22] Complementarily, from standard diode measurements to Au/N2200/Al,
142 by applying an external bias between the base and collector, V_{BC} , we observe a rectifying
143 behavior where the diode current, I_{diode} , is higher when electrons are injected by the top Al
144 layer ($V_{BC} < 0$) than when they are injected from the base gold ($V_{BC} > 0$) (see Figure S1 and
145 Supplementary Note 1). This behavior suggests the formation of a high-energy barrier at the

146 Au/N2200 interface. Figure 2b shows the $I_{C-hot}-V_{EB}$ characteristics of the device at the same
147 set of temperatures. We observe that I_{C-hot} is 4 orders of magnitude lower than I_E . This is a
148 characteristic behavior of hot electrons in semiconductors.[12] Figure 2c shows I_{C-hot} versus
149 V_{EB} at 290 K together with the linear fit of the growth of the current to the $I_{C-hot} = 0$ line.[21]
150 Using this straightforward method the energy barrier Δ between Au and N2200 is estimated to
151 be 1.2 ± 0.1 V (dotted blue arrow). We fabricated four chips containing several devices each
152 in different deposition rounds. The average barrier value measured was 1.2 ± 0.1 V. The
153 device-to-device variation in each chip is lower than the measurement precision, while the
154 maximum variation from chip to chip is 0.1V. More complex fittings that consider the
155 tunneling probability and the density of states of the semiconductor can be also employed for
156 the reproduction of the curves, but the ultimate results are in any case extremely similar.[12]
157 The dotted green arrow points out the onset of the non zero I_{C-hot} at 0.9 ± 0.1 V, which
158 corresponds to the energy barrier for charge injection into the polymer interface states.[12]
159
160 Hot electron spectroscopy provides information about the metal/semiconductor energy
161 barriers in device operative conditions as well as how this interfacial energy determines the
162 charge injection into the semiconductor. Complementary to this, in order to verify the
163 metal/semiconductor energy barrier, well established methods such as UPS can be used.^[9, 23]
164 This technique probes the ionization energies of the occupied electronic density of states
165 without the lattice relaxation energy that can occur upon photoemission of an electron (see
166 Experimental Section). **Figure 3a** shows the HeI survey scan of a N2200 film on gold. The
167 frontier edge of the occupied electronic structure is typically taken as the vertical ionization
168 potential (IP) referenced to the Fermi energy (0 eV) in the figure. To get an IP value
169 referenced to the vacuum level, the work function of the sample is determined from the so-
170 called secondary electron cut-off, **Figure 3b**. The UPS measurements carried out gave an IP
171 of 5.7 ± 0.1 eV with work functions of 4.7 ± 0.1 eV. A negative pinning energy of 3.9 ± 0.1 eV

172 (corresponding to the energy of a singly occupied LUMO at the polymer-gold interface
173 screened by the image charge of the gold surface, see Supplementary Note 2) was also
174 obtained from UPS measurements, in good agreement with Kelvin probe derived results in
175 literature.^[24] The small variation in work function (± 0.1 eV) between films is partly the
176 experimental error but also due to variation in the starting gold surface as well as film
177 formation at the Au/N2200 interface, and is in the range of previous studies of polymer-gold
178 interfaces.^[25] The electron injection barrier at the Au/N2200 interface can then be estimated
179 from the UPS values as 4.7 eV $-$ 3.9 eV = 0.8 ± 0.1 eV. However, we must consider that this
180 barrier represent injection of an electron into the edge of the N2200 n-polaron (relaxed singly-
181 occupied LUMO) distribution at the gold interface, where the image charge effect shifts the
182 energy deeper into the gap compared to the bulk n-polaron distribution (see **Figure 3c**), a
183 well-known effect from both device physics and interface energy level alignment.^[26-28] The
184 size of the shift going from interface to bulk depends on a variety of factors including the
185 organic film morphology and its dielectric constant, with values in literature ranging between
186 0.3 eV up to 0.7 eV.^[27-29] Hence, the electrons injected into the edge states are bound at the
187 interface and will not make it to the collecting contact as no driving voltage is applied (see
188 simulations below). In fact, only electrons injected near the center ($\sim 0.5 \sigma$, being σ the width
189 of the Gaussian energy disorder) of the bulk n-polaron distribution are expected to contribute
190 to the current under these conditions (see Figure 3c).^[30, 31] Taking the lower value of 0.3 eV
191 for the image charge induced shift between interface and bulk we get a total barrier for the
192 conditions of ballistic injection current in the device as 0.8 eV + 0.3 eV = 1.1 eV. Both the
193 interface energy barrier and bulk energy barrier values are in good agreement with the direct
194 experimental observation performed by in-device hot electron spectroscopy, albeit if several
195 approximation have been needed for the extraction of the bulk energy barrier.

196

197 UPS measurements show a change in the work function of the gold contact coming from its
198 air exposure, which is a well-known experimental result reported extensively in literature
199 (Figure 3b and Ref. 16). However, it is not clear if such contamination layer might modulate
200 the energy barrier values when these are measured by in-device hot electron spectroscopy. In
201 order to disentangle this question, we fabricate a hot electron device in which the gold
202 interface is cleaned with oxygen plasma for 5 minutes just before the spin coating of the
203 polymer. **Figure 3d** shows the measured hot-electron current normalized to $I_{C-hot}/I_{C-hot(max)}$ as
204 a function of the applied bias V_{EB} at 290 K corresponding to both samples, one with clean
205 gold (black line) and a standard device with untreated gold (red line). $I_{C-hot(max)}$ corresponds to
206 the maximum value of the measured hot-electron current. No difference in the energy barrier
207 value is observed when we compare both samples, indicating that a contamination layer
208 coming from air exposure of gold does not affect substantially the carrier injection in
209 agreement with UPS literature on gold/polymer contacts.^[32]

210

211 For a better understanding of our results we have developed a theoretical model for the hot-
212 electron transistor. The model is kept simple but includes the different parts of the device as
213 illustrated in **Figure 4a**. The central part is the polymer film, represented as hopping sites
214 (balls), which is sandwiched between gold and aluminum electrodes. Hot-carriers can be
215 injected with a rate ν through the base into the polymer as illustrated by black arrows in
216 Figure 4a. The charge transport in the polymer is modeled as hopping transport between
217 localized states (sticks between balls), while electron transfer from Au (Al) into the polymer
218 and back is possible via the Au (Al) Fermi level. We solve the Poisson equation and transport
219 Master equation simultaneously (see Experimental Section for details) for a steady state.

220

221 In the simulations, we assume hot carrier operation conditions by setting $V_{BC} = 0V$ ($\Phi = 0$ eV
222 is the metal Fermi level). When no hot electrons are provided at the base ($\nu = 0$), we expect
223 the electron affinity of the polymer interface states, which is increased by an image charge of
224 0.3 eV, to be at 3.8 eV (i.e. $\Phi = 0.9$ eV). This choice for the energy level of the lowest polymer
225 states at 0.1 eV above the pinning onset of 3.9 eV is due to interfacial energetic disorder and
226 finite temperature which leads to the onset of charging of the lowest polymer states (pinning)
227 at such offset. When hot electrons are provided with a finite rate ν and $V_{EB} = -1.2$ V, the
228 solution of the equations yields the potential distribution shown in **Figure 4b**. The resulting
229 potential is dominated by the built-in potential and the image-charge potential close to the
230 Au/N2200 interface. In addition, a small space-charge contribution close to the interface
231 occurs at the chosen injection conditions.

232

233 **Figure 4c** summarizes the calculated I_{C-hot} for varying V_{EB} . At small hot-electron energy
234 ($|V_{EB}| \leq 1.1$ V) the electrons can hardly reach the transport levels of the bulk polymer although
235 the lowest polymer states close to the interface may be populated, i.e. electrons cannot escape
236 the barrier from the image-charge and I_{C-hot} is suppressed. This barrier can be overcome by
237 further increasing $|V_{EB}|$, which provides more electrons with higher energies. Note that the
238 hot-electrons arrive with energies continuously distributed between zero and $|V_{EB}|$. This leads
239 to the current onset at $V_{EB} = -1.2$ eV (from a linear fit) and further linear increase in I_{C-hot} .
240 These results are in good agreement with the ones obtained by in-device hot electron
241 spectroscopy.

242

243 In conclusion, we have shown that in-device hot electron spectroscopy is a reliable and
244 straightforward method for the determination of metal/polymeric semiconductor energy
245 barriers, making their use convenient for the engineering of commercial ex-situ fabricated

246 organic electronic devices. Our research also makes in-device hot electron spectroscopy a
247 handy tool for the general research community working in organics, as its use is available for
248 laboratories, which do not use ultra-high vacuum evaporation systems. Our results are
249 confirmed by an established technique such as UPS. This shows to be a reliable, but non-
250 direct, method for the determination of interfacial transport energy barriers, thus highlighting
251 the importance of our direct method. Along the article we have also explored the role of the
252 contamination layer coming from the air exposure of the devices in the fabrication process,
253 we have seen that it does not play a significant role. Our experimental work has been
254 complemented by a theoretical model developed for transport in hot electron devices. This
255 model has given a further understanding on the role of the interfaces in hot electron devices as
256 well as highlighting the existing differences between the two techniques employed. This work
257 gives a new approach to the study of metal/polymeric semiconductor interfaces as well as
258 providing a new design tool for organic electronics.

259
260

261 **Experimental Section**

262 *Device fabrication:* All metallic parts of the devices described in this work were fabricated
263 in ultra high vacuum (UHV) evaporator chamber (base pressure $<10^{-9}$ mbar) with a shadow
264 mask system. Metals (99.95%) (Lesker) were evaporated by e-beam at a rate of 0.1 nm s^{-1} .

265
266 The organic layer was ex-situ spin coated in clean room at ambient conditions. The solution
267 was prepared with 5mg of N2200 ($> 99.5\%$) (PolyeraActivInkTM) dissolved in 1 ml of CHCl_3
268 (99.9%)(extra dry, stabilized) (AcroSeal). $90 \mu\text{l}$ of this solution were spin coated on the
269 sample for 60s at 4000 rpm. In order to evaporate the residual solvent in the sample before the
270 evaporation of the top metallic contact, this was kept in vacuum (10^{-6} mbar) for two hours.

271

272 *Electrical characterization:* Electrical characterization was performed under high vacuum
273 (base pressure 5×10^{-5} mbar) in a variable-temperature probe-station (Lakeshore). A Keithley
274 4200 semiconductor analyzer system was used to record I - V curves.

275

276 *Photoelectron spectroscopy:* Measurements were carried out in a UHV surface analysis
277 system equipped with a Scienta-200 hemispherical analyzer. The base pressure of the sample
278 analysis chamber was 2×10^{-10} mbar. UPS was performed using a standard He-discharge
279 lamp with HeI 21.22 eV as excitation source and an energy resolution of 50 meV. Radiation
280 damage was tested for and found not to occur. The work functions were derived from the
281 secondary electron cut-off, and XPS was measured using monochromatized Al Ka with $h\nu =$
282 1486.6 eV. All measurements were calibrated by referencing to the Fermi level and Au 4f_{7/2}
283 peak position of an Ar⁺ ion sputter-clean gold foil.

284

285 *Modeling:* All device simulations are based on a master equation approach taking into account
286 the electric field distribution through the solution of the 1D Poisson equation, the image
287 charge potential, a random disorder potential of $\sigma = 0.1$ eV at the interfaces and the built-in
288 potential coming from the different work functions of the electrodes.^[33] The tunneling rates of
289 the hot electrons into the polymer layer decay exponentially away from the Au surface.
290 Miller-Abraham hopping rates are used between sites within the polymer and for the hopping
291 between the polymer and the Au and Al levels.^[34] To calculate the hot-electron current, we
292 note that the hot electrons from the base enter the polymer region with energy equal or below
293 $-eV_{EB}$ and can contribute to the current I_{C-hot} . Therefore, I_{C-hot} is obtained from integrating
294 these contributions up to $-eV_{EB}$.

295

296

297

298 **Supporting Information**

299 Supporting Information is available from the Wiley Online Library or from the author.

300

301

302 **Acknowledgements**

303 This work is supported by the European Research Council (257654-SPINTROS), by the

304 Spanish MINECO under Project No. MAT2015-65159-R, and by the Basque Government

305 (under Project No. PC2015-1-01. A.A. acknowledges the Basque Government for a PhD

306 fellowship (PRE_2015_2_0139).

307

308

309 Received: ((will be filled in by the editorial staff))

310 Revised: ((will be filled in by the editorial staff))

311 Published online: ((will be filled in by the editorial staff))

312

313

314 **References**

315 [1] S. Holliday, R. S. Ashraf, A. Wadsworth, D. Baran, S. A. Yousaf, C. B. Nielsen, C.-H.

316 Tan, S. D. Dimitrov, Z. Shang, N. Gasparini, M. Alamoudi, F. Laquai, C. J. Brabec, A. Salleo,

317 J. R. Durrant, I. McCulloch, *Nat. Commun.* **2016**, *7*, 11585.

318 [2] J. Lee, H.-F. Chen, T. Batagoda, C. Coburn, P. I. Djurovich, M. E. Thompson, S. R.

319 Forrest, *Nat. Mater.* **2015**, *15*, 92.

320 [3] M. Muccini, *Nat. Mater.* **2006**, *5*, 605.

321 [4] S. R. Forrest, *Nature* **2004**, *428*, 911.

322 [5] R. H. Friend, R. W. Gymer, A. B. Holmes, J. H. Burroughes, R. N. Marks, C. Taliani,

323 D. D. C. Bradley, D. A. Dos Santos, J. L. Bredas, M. Lögdlund, W. R. Salaneck, *Nature* **1999**,

324 *397*, 121.

325 [6] M. F. Lo, T. W. Ng, T. Z. Liu, V. A. L. Roy, S. L. Lai, M. K. Fung, C. S. Lee, S. T.

326 Lee, *Appl. Phys. Lett.* **2012**, *96*, 113303.

327 [7] H. Sirringhaus, *Adv. Mater.* **2005**, *17*, 2411.

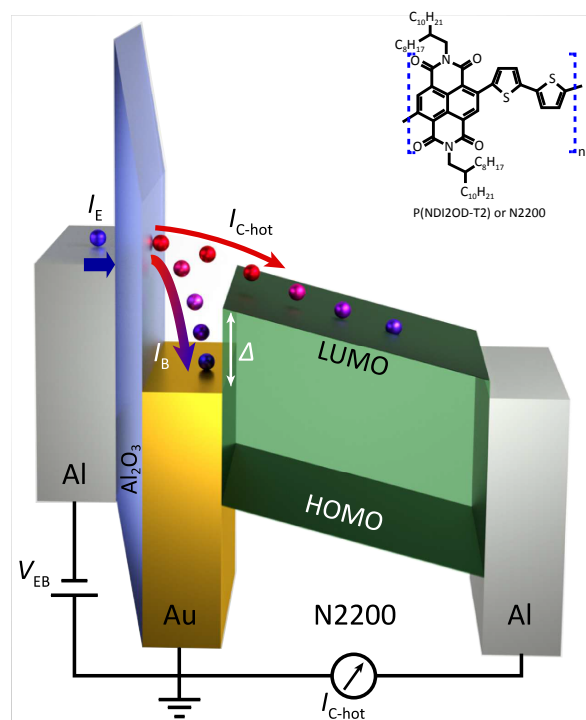
328 [8] J. Hwang, A. Wan, A. Kahn, *Materials Sci. Eng. R* **2009**, *64*, 1.

- 329 [9] B. S. Braun, W. R. Salaneck, M. Fahlman, *Adv. Mater.* **2009**, *21*, 1450.
- 330 [1] S. Holliday, R. S. Ashraf, A. Wadsworth, D. Baran, S. A. Yousaf, C. B. Nielsen, C.-H.
331 Tan, S. D. Dimitrov, Z. Shang, N. Gasparini, M. Alamoudi, F. Laquai, C. J. Brabec, A. Salleo,
332 J. R. Durrant, I. McCulloch, *Nat. Commun.* **2016**, *7*, 11585.
- 333 [2] J. Lee, H.-F. Chen, T. Batagoda, C. Coburn, P. I. Djurovich, M. E. Thompson, S. R.
334 Forrest, *Nat. Mater.* **2015**, *15*, 92.
- 335 [3] M. Muccini, *Nat. Mater.* **2006**, *5*, 605.
- 336 [4] S. R. Forrest, *Nature* **2004**, *428*, 911.
- 337 [5] R. H. Friend, R. W. Gymer, A. B. Holmes, J. H. Burroughes, R. N. Marks, C. Taliani,
338 D. D. C. Bradley, D. A. Dos Santos, J. L. Bredas, M. Lögdlund, W. R. Salaneck, *Nature* **1999**,
339 *397*, 121.
- 340 [6] M. F. Lo, T. W. Ng, T. Z. Liu, V. A. L. Roy, S. L. Lai, M. K. Fung, C. S. Lee, S. T.
341 Lee, *Appl. Phys. Lett.* **2012**, *96*, 113303.
- 342 [7] H. Sirringhaus, *Adv. Mater.* **2005**, *17*, 2411.
- 343 [8] J. Hwang, A. Wan, A. Kahn, *Materials Sci. Eng. R* **2009**, *64*, 1.
- 344 [9] B. S. Braun, W. R. Salaneck, M. Fahlman, *Adv. Mater.* **2009**, *21*, 1450.
- 345 [10] S. Parui, A. Atxabal, M. Ribeiro, A. Bedoya-Pinto, X. Sun, R. Llopis, F. Casanova, L.
346 E. Hueso, *Appl. Phys. Lett.* **2015**, *107*, 183502.
- 347 [11] T. R. Ohno, Y. Chen, S. E. Harvey, G. . Kroll, J. H. Weaver, *Phys. Rev. B* **1991**, *44*,
348 13747.
- 349 [12] M. Gobbi, L. Pietrobon, a Atxabal, a Bedoya-Pinto, X. Sun, F. Golmar, R. Llopis, F.
350 Casanova, L. E. Hueso, *Nat. Commun.* **2014**, *5*, 4161.
- 351 [13] J. S. Jiang, J. E. Pearson, S. D. Bader, *Phys. Rev. Lett.* **2011**, *106*, 156807.
- 352 [14] P. I. Djurovich, E. I. Mayo, S. R. Forrest, M. E. Thompson, *Org. Electron.* **2009**, *10*,
353 515.
- 354 [15] H. Yan, Z. Chen, Y. Zheng, C. Newman, J. R. Quinn, F. Dötz, M. Kastler, A.

- 355 Facchetti, *Nature* **2009**, *457*, 679.
- 356 [16] C. Mu, P. Liu, W. Ma, K. Jiang, J. Zhao, K. Zhang, Z. Chen, Z. Wei, Y. Yi, J. Wang,
357 S. Yang, F. Huang, A. Facchetti, H. Ade, H. Yan, *Adv. Mater.* **2014**, *26*, 7224.
- 358 [17] M. Caironi, M. Bird, D. Fazzi, Z. Chen, R. Di Pietro, C. Newman, A. Facchetti, H.
359 Sirringhaus, *Adv. Funct. Mater.* **2011**, *21*, 3371.
- 360 [18] S. Parui, B. Wit, L. Bignardi, P. Rudolf, B. Kooi, B. J. Van Wees, T. Banerjee, *Appl.*
361 *Phys. Lett.* **2011**, *99*, 32104.
- 362 [19] N. Balkan, in *Hot Electrons Semicond.*, Clarendon Press, Oxford, **1998**, pp. 385–427.
- 363 [20] W. J. Kaiser, L. D. Bell, *Phys. Rev. Lett.* **1988**, *60*, 1406.
- 364 [21] L. D. Bell, W. J. Kaiser, *Phys. Rev. Lett.* **1988**, *61*, 2368.
- 365 [22] X. Sun, M. Gobbi, A. Bedoya-pinto, O. Txoperena, F. Golmar, R. Llopis, A. Chuvilin,
366 F. Casanova, L. E. Hueso, *Nat. Commun.* **2013**, *4*, 2794.
- 367 [23] B. H. Ishii, K. Sugiyama, E. Ito, K. Seki, *Adv. Mater.* **1999**, *11*, 605.
- 368 [24] I. Lange, J. C. Blakesley, J. Frisch, A. Vollmer, N. Koch, D. Neher, *Phys. Rev. Lett.*
369 **2011**, *106*, 216402.
- 370 [25] S. Braun, M. P. De Jong, W. Osikowicz, W. R. Salaneck, *Appl. Phys. Lett.* **2007**, *91*,
371 202108.
- 372 [26] Q. Bao, S. Fabiano, M. Andersson, S. Braun, Z. Sun, X. Crispin, M. Berggren, X. Liu,
373 M. Fahlman, *Adv. Funct. Mater.* **2016**, *26*, 1077.
- 374 [27] L.-H. Zhao, R.-Q. Png, C. C. H. Chiam, H. Guo, J.-M. Zhuo, L.-L. Chua, A. T. S. Wee,
375 P. K. H. Ho, *Appl. Phys. Lett.* **2012**, *101*, 53304.
- 376 [28] L. Lindell, C. Vahlberg, K. Uvdal, M. Fahlman, S. Braun, *J. Electron Spectros. Relat.*
377 *Phenomena* **2015**, *204*, 140.
- 378 [29] X.-Y. Zhu, *J. Phys. Chem. B* **2004**, *108*, 8778.
- 379 [30] W. C. Germs, J. J. M. van der Holst, S. L. M. van Mensfoort, P. A. Bobbert, R.
380 Coehoorn, *Phys. Rev. B* **2011**, *84*, 165210.

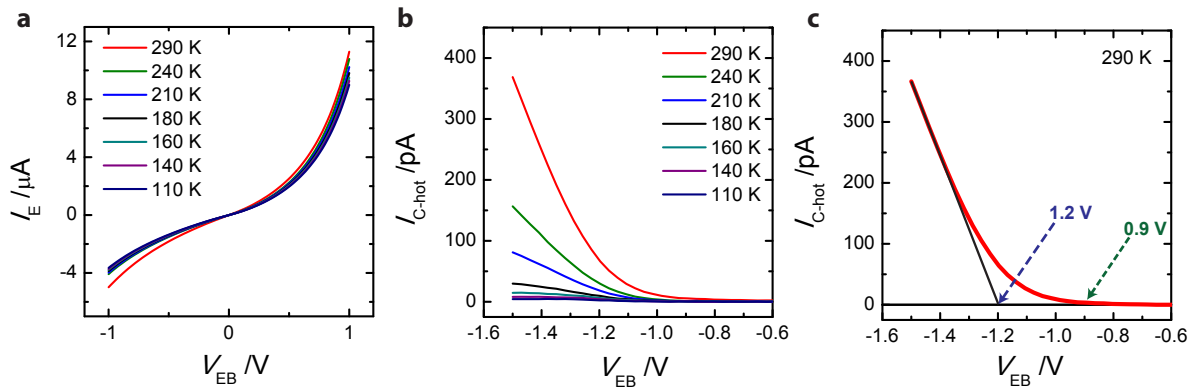
- 381 [31] J. Cottaar, L. J. A. Koster, R. Coehoorn, P. A. Bobbert, *Phys. Rev. Lett.* **2011**, *107*,
382 136601.
- 383 [32] W. Osikowicz, M. P. de Jong, S. Braun, C. Tengstedt, M. Fahlman, W. R. Salaneck,
384 *Appl. Phys. Lett.* **2006**, *88*, 193504.
- 385 [33] J. J. M. van der Holst, M. A. Uijtewaal, B. Ramachandhran, R. Coehoorn, P. A.
386 Bobbert, G. A. de Wijs, R. A. de Groot, *Phys. Rev. B* **2009**, *79*, 85203.
- 387 [34] A. Miller, E. Abrahams, *Phys. Rev.* **1960**, *120*, 745.
- 388
- 389
- 390
- 391
- 392
- 393
- 394
- 395
- 396
- 397
- 398
- 399
- 400
- 401
- 402
- 403
- 404
- 405

406
407
408
409
410
411
412
413
414
415
416



417 **Figure 1.** Scheme of the working principle and the energy levels of the device in rigid band
418 approximation. The tunneling current I_E flows from the emitter to the base when a negative
419 bias V_{EB} is applied at the emitter/base terminals. A major part of this injected current is
420 attenuated in the base and collected as I_B while the other part of I_E flows ballistically to the
421 base/collector interface. When the bias V_{EB} is higher than Δ , a fraction of the I_E flows into the
422 N2200 and is measured as I_{C-hot} . This current is collected without any external bias applied
423 between the base and the collector terminals. Inset: chemical structure of P(NDI2OD-T2) or
424 N2200 polymer.

425
426



427
 428 **Figure 2.** Electrical characterization of the device. a) Temperature dependence of the emitter
 429 current I_E measured at two terminals in the Al/AlOx/Au tunnel junction as a function of
 430 applied bias V_{EB} . b) Temperature dependence of the hot-electron current $I_{C\text{-hot}}$ measured in the
 431 Au/N2200/Al stack as a function of the applied bias V_{EB} . c) $I_{C\text{-hot}}$ measured as a function of
 432 the applied bias between the emitter and the base V_{EB} at 290 K and the linear fit to $I_{C\text{-hot}} = 0$ to
 433 obtain the barrier height Δ .

434

435

436

437

438

439

440

441

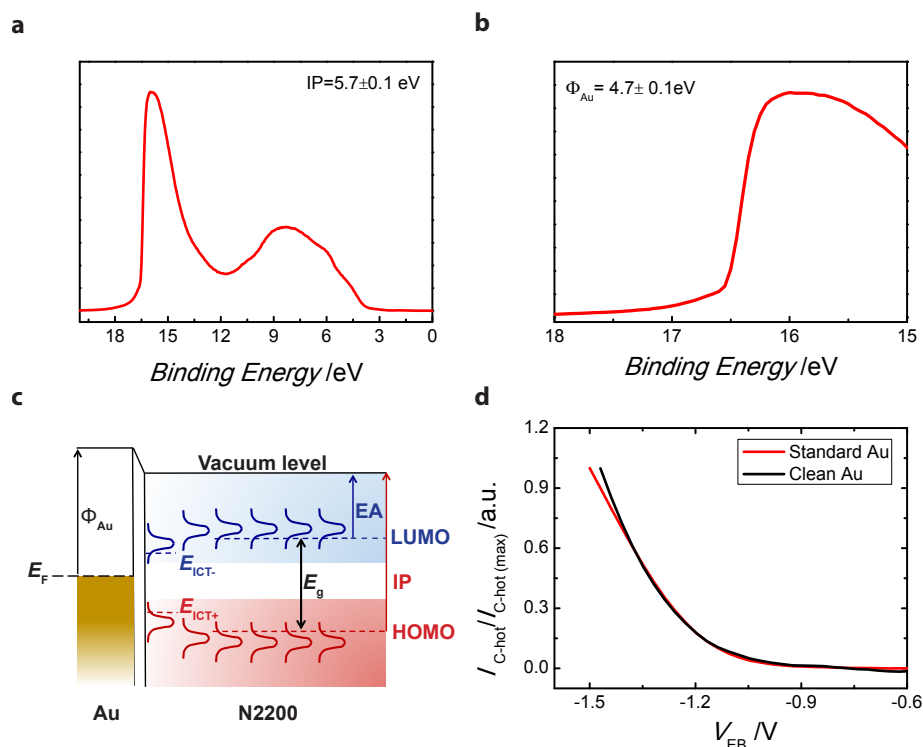
442

443

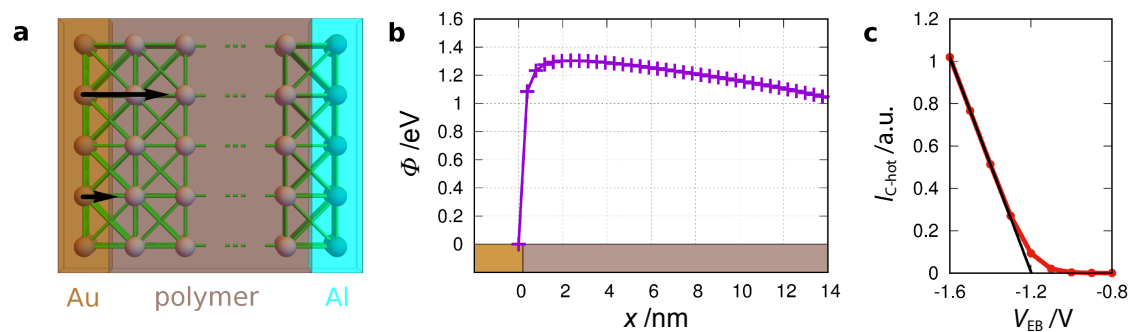
444

445

446



447
 448 **Figure 3.** Comparison of UPS and hot-electron measurements for standard and clean gold. a)
 449 Ionization potential of the N2200 measured with UPS (Ultraviolet Photoemission
 450 Spectroscopy). A 90-nm-thick N2200 layer is spin coated on Au (14 nm)/AlOx (20 nm)/SiOx
 451 (200 nm)/Si. b) Work function of gold measured with UPS. The gold is deposited on top of
 452 AlOx (20 nm)/SiOx (200 nm)/Si and is covered with 90 nm of N2200. c) Au/N2200 interface
 453 energy diagram. E_F is the Fermi energy and Φ_{Au} the work function of gold. LUMO
 454 corresponds to the lowest unoccupied molecular orbital, HOMO to the highest occupied
 455 molecular orbital, IP to the ionization potential, EA to the electron affinity and E_g to the
 456 energy band gap of the N2200 polymer. The integer charge transfer states are represented as
 457 E_{ICT+} and E_{ICT-} . d) Measured hot electron current normalized to $I_{C-hot} / I_{C-hot(max)}$ as a function
 458 of the applied bias V_{EB} at 290 K. $I_{C-hot(max)}$ corresponds to the maximum value of the measured
 459 hot electron current. The red curve corresponds to the standard device with non-clean base
 460 gold and the black curve corresponds to oxygen-plasma-cleaned base gold device.
 461



462

463 **Figure 4.** Theoretical model for the experimental data. a) Structural model of the
464 Au/N2200/Al heterostructure. The polymer is represented electronically by hopping sites
465 (indicated by balls in the central region), which are connected by hopping rates (sticks). b)
466 Energy levels as a function of distance x to the Au surface, calculated from the electrostatic
467 potential (for $V_{EB}=-1.2$ V). c) Simulated hot-electron current-voltage characteristics (red) and
468 extrapolation of threshold voltage to -1.2 V (black).

469

470

471 **In this work we demonstrate in-device hot electron spectroscopy as a direct and reliable**
472 **technique for the determination of the energy barrier between a metal and a solution-**
473 **processed electron-transporting organic semiconductor.** With our experimental advance, we
474 open new possibilities to bring this technique closer to the organic electronics industry.

475
476 **Keywords: Hot electron transistor, spectroscopy, energy barrier, polymer, organic**
477 **electronics**

478
479 Ainhoa Atxabal, Slawomir Braun, Thorsten Arnold, Xiangnan Sun, Subir Parui, Xianjie Liu,
480 Cristian Gozalvez, Roger Llopis, Aurelio Mateo-Alonso, Felix Casanova, Frank Ortman,
481 Mats Fahlman, Luis E. Hueso*

482
483 **Energy Level Alignment at Metal/Solution-Processed Organic Semiconductor Interfaces**
484
485

